11th International Conference on Fracture Mechanics of Concrete and Concrete Structures
FraMCoS-11
J. M. Chandra Kishen, A. Ramaswamy, S. Ray and R. Vidyasagar (Eds)
https://doi.org/10.21012/FC11.092339

INFLUENCE OF INTER-LAYER INTERFACES ON FRACTURE BEHAVIOR OF 3D PRINTED CONCRETE

SPANDANA PARITALA[*], TIPPABHOTLA KAMAKSHI[*], AND KOLLURU V.L. SUBRAMANIAM [†]

[*]Indian Institute of Technology Hyderabad
Civil Engineering, I.I.T. Hyderabad,
Kandi, Sangareddy, Telangana - 502284, India
† Indian Institute of Technology Hyderabad
Civil Engineering, I.I.T. Hyderabad,
Kandi, Sangareddy, Telangana - 502284, India
e-mail: KVLS@ce.iith.ac.in, www.iith.ac.in/ce/kvls/

Key words: Fracture; layered composite; interface; Bond; 3D Concrete Printing.

Abstract: Extrusion-based layer deposition is the most popular form of 3D Concrete Printing (3DCP). A 3D printed assembly is a composite made up of multiple layers. The stress response of the printed assembly is influenced by the directionality of the material deposit and the stress transfer between the layers. The bond between the layers determines the level of stress transfer and the composite action achieved in printed assemblies. The inter-layer bonding is an important parameter, which effects the homogeneity of the element and thus its mechanical behavior. The bond between the layers depends upon several factors including the fluidity of the mixture and the time between layers. Weak interfaces develop between two adjacent layers of concrete depending on the fluidity of the mix and the time gap between placement. The study involves the understanding of interface between the layers on the fracture behavior of the printed beams. Crack propagation in the layered beam is evaluated using digital image correlation. The influence of changes in the interface created by different wait times on the crack planes across the printed interfaces are studied. The reduction in the bond between layers with waiting time is related to fracture behavior of the printed beam.

1 INTRODUCTION

3D concrete printing (3DCP) is an additive manufacturing technology, that has emerged as a booming method of construction, with significant research accomplishments and extensive industrial applications in the recent years. Among various types of concrete additive manufacturing techniques, Extrusion-based 3DCP, the method of layer-by-layer concrete deposition as per the designed print paths has greater potential to create large scale elements, without the requirement of formwork. 3DCP has great capability in enhancing the freedom of architectural design and accuracy of construction, reducing the waste production and labour expenses, eliminating formwork usage, and achieving faster rate of construction. The application of 3D printed concrete is not just limited to architectural components, but also buildings [1], bridges [2], permanent formwork [3], connecting zones [4], topology optimized structures [5], functional graded structures [6] and many other new and innovative applications. The properties of 3DCP materials have been the subject of recent studies. The rheological properties [7] and fresh characteristics have been shown to have a significant impact on the later-age properties [8–10]. Other properties such as

mechanical properties [11,12], durability [13], shrinkage [14], and fire response [15] have also been investigated.

A 3D printed assembly formed by layer-by-layer extrusion process can be seen as a composite comprising multiple stacked layers. Its overall properties depend on the material properties resulting from the extrusion process and the effectiveness of stress transfer between the layers. Achieving the required level of composite action requires adequate stress transfer between the printed layers. The interlayer bond strength in 3D concrete printing (3DCP) significantly influences the mechanical strength and durability of the printed elements. The process of layer-by-layer deposition arises some new challenging factors which cause the formation of a weak interfacial bond between the adjacent printed layers.

To predict the structural capacity of the 3D printed elements, it is very essential to have a proper understanding of the stress transfer within the printed elements. If the adhesion between two layers is not adequate, it causes a poor bonding between those layers, which is result in the formation of a "Cold joint". As the rheology of the fresh concrete being deposited during printing is time dependent, the microstructure of the interface is significantly influenced by concrete rheology [16,17]. Along with rheological properties (especially high thixotropy), the factors which influence the cold joint formation are time gap between the layer deposition, surface moisture, interfacial voids, nozzle standoff distance, print speed, and others which have been highlighted in earlier studies [7,12,18,19].

Generally, the time gap between two adjacent layers should be sufficient to let the bottom layer get adequately hardened to withstand the weight of the subsequent layer being deposited, as well as the time within which it is still fresh to form a good bond with that subsequent layer [20]. It is crucial to consider the influence of time gap between the layers, extrusion-based 3D concrete printing involves printing of larger-scale structural components, which can result in the requirement of longer print time gaps between the deposition of two adjacent layers. The time gap between the printed can be in the order ranging from seconds to minutes depending upon the scale and design of the element. For example, RC beam (4 m x 0.45 m x 0.25 m) fabricated with 3DCP technology had the interlayer time gap of approximately 50–90 sec. depending on the shape of the segment [21]. The elements (3.5 m × 1 m × 0.9 m) used for a 3D printed pedestrian bridge had an interlayer time gap of approximately 5 min. and 20 sec. [22]. A 2-story residential house (38 m2) printed by COBOD had an interlayer time gap ranging from 7 min. to 15 min. [23].

Increase of print time gap between the layers can lead to the occurrence of air pockets and voids at the interface [24]. The cohesion between printed layers is significantly affected by two key factors: the fluidity of the mixture and the time interval between adjacent layers. While a longer time gap promotes the development of static yield stress, which improves the buildability of the assembly, it concurrently leads to a reduction in bond strength. Adjusting the time gap between subsequent layers plays a crucial role in the inter-layer bond in printed structures [25,26]. Previous research indicates that subjecting the deposited layer to prolonged exposure in a dry atmosphere can lead to a notable reduction in bond strength. To improve bond strength over prolonged periods, it has been suggested that protecting the exposed layer from drying could be an effective strategy [27,28]. Nonetheless, it's worth noting that the moisture present in the deposited layers is also heavily influenced by factors such as temperature and humidity. Studies have found that increasing the time gap between printed layers leads to a reduction in the interlayer tensile strength of the elements, by observing by load capacity when subjected to a Uniaxial tension test [7,18,26].

This research assesses the influence of interlayer bonding on the fracture behavior of a printed assembly. The study involves changing the time intervals between layers to investigate the formation of cold joints within the printed assembly. By increasing the time gap between

printed layers, a cold joint is intentionally introduced. To examine the effects of this cold joint, the researchers analyse the crack propagation in the printed assembly using Digital Image Processing (DIC) to obtain full-field displacement measurements.

2 EXPERIMENTAL PROGRAM

In this study, a cement-based mixture composed of Birla A1 Strongcrete^{TM} cement was utilized for 3D printing. The cement used was categorized as OPC 53 grade, in accordance with the standards of IS12269:2013 [29]. The water-to-cement ratio and the sand-to-cement ratio were maintained at 0.32 and 1:1, respectively. This mixture included Natural sand that adheres to Zone-2 specifications, as outlined in IS 383-2016 [30]. To enhance the material properties, a small content of approximately 0.12% of micro poly-propylene fibers with an aspect ratio of 800 was incorporated into the mixture. The 3D printing process was performed using a 6-degree freedom robotic arm printer provided by the ABB group. The printer utilized a circular nozzle with a diameter of 25 mm, a print speed of 350 mm/s, and a flow rate of 30 lit/min. The printed specimens' dimensions were 500 mm X 150 mm X 100 mm. Each specimen consists of 50 mm layer width, and have a total height of 150 mm. Figure 1 illustrates the schematic representation of a typical printed specimen with the designated print directions. The time interval between each layer in the 3D printed specimen was approximately 4 seconds.

Print time gap represents the time required to complete one layer while printing an object. Specimens were printed with different time gaps indicated as the ‘0-minute’, 9-minute’ and the 20-minute’ specimens. The "0-minute" specimen involves printing 10 layers, each with a height of 15 mm, without any pauses in between. Each layer was printed with a time gap of 4 seconds. The 9-minute and 20-minute specimen were printed of six 15 mm layers with 9 and 20-minute gaps, respectively between the second and third layers. During this pause, the second layer was left exposed to the ambient environment without any covering. After the 9 or 20-minute intervals, the printing process was resumed, and the subsequent layers were printed continuously. The interface between the second and third layers printed after 9 and 20 minutes is referred to as the 9 and 2—minute interface, respectively. Following the printing process, the specimens were placed in covered in wet burlap cured in the laboratory environment.

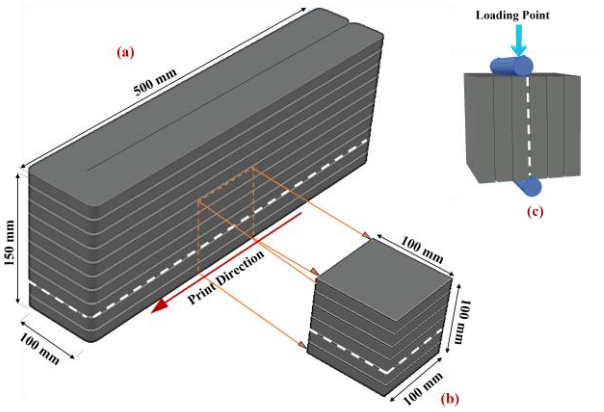

Fig.1. The schematic of a typical printed specimen with the print directions

The tensile strength of the interface between the layers was determined using split tensile testing. Specimens for tensile were cut from the printed beams across the 0 and 9-minute interfaces. Cube specimens of dimensions 100 mm were loading along the interface between layers. The specimen was loaded along the 9-minute interface. The loading setup for tensile strength conformed to IS 5816 [33]. The tensile strengths of the interfaces were 1.65 and 0.9 MPa for the 0 and 9-minute interfaces.

Fracture testing was conducted on beams cut from the printed specimens. Flexure tests were

conducted in a three-point bending setup using a servo-hydraulic closed-loop test machine, following the guidelines of EN 14651:2005 [32]. A 20 mm notch was introduced at the mid-span of the beam, and a Crack Mouth Opening Displacement (CMOD) gauge was attached across the notch. The beams were subjected to testing with an effective span of 450 mm, and the CMOD was controlled at a rate of 0.5 µm/s.

The front face of the test specimen was prepared for digital image correlation (DIC) with a sprayed-on speckle pattern. A white background was applied and a random speckle pattern on the surface is made using a mist of black spray. Images of the specimen were collected during the fracture test using a digital camera of 5 miegapixel resolution. A schematic of the test setup is shown in Figure.2. The digital images captured during the flexure test were used for image correlation, which allowed for the determining the full-field displacements on the surface of the beam.

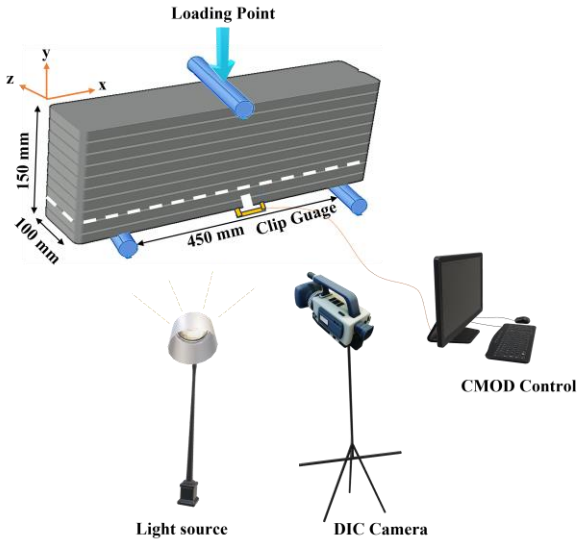

Fig.2. Illustration of the Flexural testing and DIC setup

3 RESULTS AND DISCUSSIONS

The initial setting time of determined using Vicat Apparatus was found to be 200 minutes. Hence the initial setting time of cement is significantly greater than the provided time gap of printing of 20 min for the 20- minute specimen. The initial setting time determined by Vicat Apparatus was 200 minutes. This indicates that the time it takes for the initial setting time of cement is considerably longer than the 20-minute printing time gap specified for the 20-minute specimen.

The printed material exhibited varying compressive strengths along different directions: 48.3 MPa (with a standard deviation of 7.82 MPa) in the Y direction, 44.66 MPa (with a standard deviation of 5.69 MPa) in the Z direction, and 38.62 MPa (with a standard deviation of 6.07 MPa) in the X direction. This disparity in compressive strength across the three directions confirms its anisotropic behavior, resulting from the layered structure of the material.

Figure.3 presents the typical fracture test response of the 0-minute beam and the strain contours in the X-direction (ε_{xx}) at various points during the load response. The layers are indicated by the markings on the edge of the contour plots. Notably, the ε_{xx} contours exhibit intense localization within the second layer of the beam, in the pre-peak phase of the load response at 6.6 kN, indicating the formation of a crack originating from the notch. Subsequently, the crack propagated throughout the depth of the beam, steadily increasing with the applied load up to the peak load of 7.83 kN. The crack had propagated across the second interface the crack tip was positioned between the second and third layers. There was contiuned progression of the crack traversing several interfaces in a predominantly vertical path along the depth of the beam in the post peak load response. There

was no apparent indication of any deviation at the inter-layer interfaces, suggesting a cohesive composite action within the layered structure. The 0-miute specimen exhibited a well-established composite action of the layered structure, affirming good bonding between the layers due to continuous printing without any time gaps.

Figure.4 presents the typical fracture test response of the 9-minute beam and the ε_{xx} and ε_{xx} strain contours at various points during the load response. The 9-minute interface ins indicated by the black line in the contour plots.

The crack initiation from the notch is occurred in the pre-peak load response. The crack extended close to the 9-minute interface in the pre-peak load response. There is a noticeable deviation in the crack path produced by crack deflection along the interface. The deflection is produced at the 9-minute interface. The crack deflects along the interface and then kinks out of the interface. The crack continues to grow into the layers deposited above the 9-minute interface in the post-peak load resp onse. The contibued crack growth in the layered structure above the 9-minute interface was predominantly vertical, traversing several interfaces.

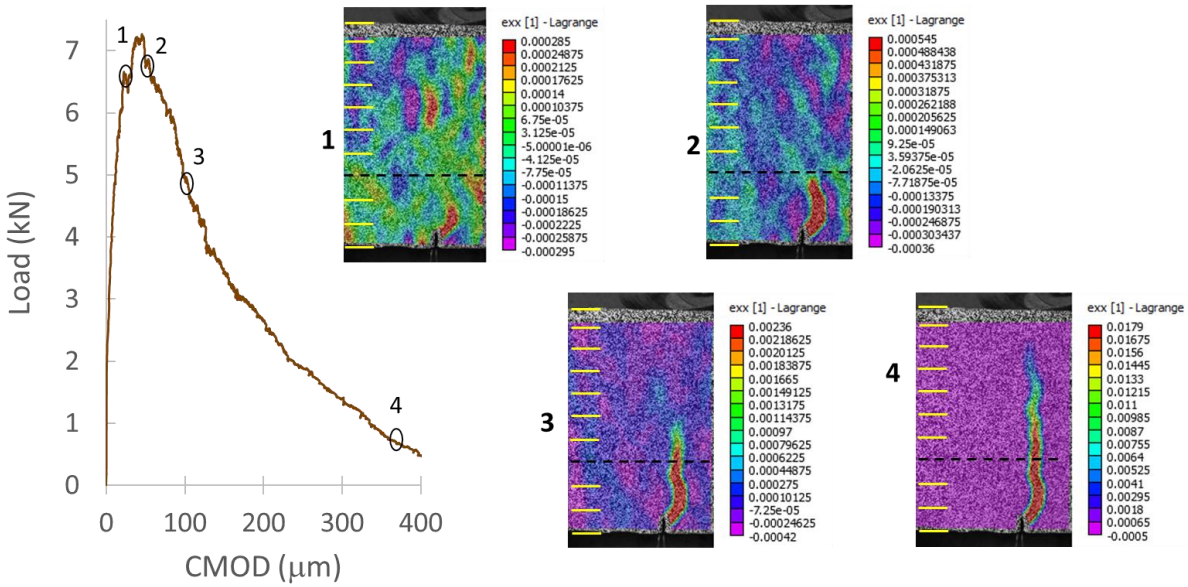

Fig.3. Load – CMOD response and the strain contours for a 0-minute specimen. The interfaces between layers of 15 mm thickness are marked on the sides of the contour plots.

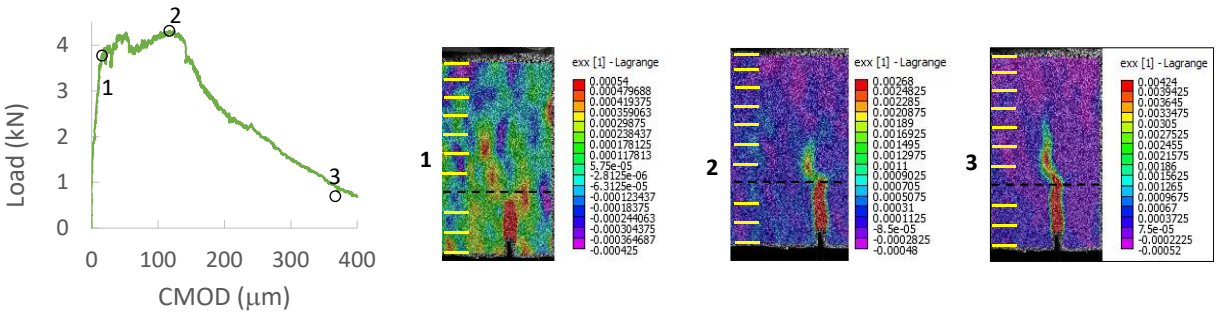

Fig.4. Load – CMOD response and the strain contours for a 9-minute specimen. The interfaces between layers of 15 mm thickness are marked on the side. The 9-minute interface is shown as a dark line.

FRACTURE ANALYSIS

The propagation of the crack at the interface betweeen two materials has the possibility of deflection or penetration at the interface, which is determined by the energy release rate ratio of the interface and matrix, Γ

$$\Gamma = \frac{G_{int}}{G_m} = \Gamma(\alpha, \beta) \tag{1}$$

where α and β are Dundur's parameters given as

$\alpha = [\mu_1(1-\nu_2) - \mu_2(1-\nu_1)] / [\mu_1(1-\nu_2) + \mu_2(1-\nu_1)]$

$\beta = [\mu_1(1 - 2\nu_2) - \mu_2(1-2\nu_1)] / [\mu_1(1-\nu_2) + \mu_2(1 - \nu_1)]$

The crack branching and propagation are shown to be influenced by a while b has a secondary influence. Considering the possibility of crack branching at the interface, as shown in Figure 4, the Γ is plotted as a function of a. There is a possiblity of double branching at the interface and the Γ for doubly deflected crack is also presented. Considering similar material across the interface, as in the case of the printed layers, the Γ is approximately ¼ and 1/8 for the singly and doubly-deflected crack, respectively.

The condition for crack growth along the interface were developed by He and Hutchinson (1989) and are given as

$$\frac{G_{intc}}{G_{mc}} < \frac{1}{4}(singly\ deflected \quad or \quad \frac{1}{8}\ (doubly\ delfected) \tag{2}$$

and $G_{int} > G_{intc}$ (3)

where G_{mc} and G_{intc} are the critical energy release rates of the material and the interface, respectively.

The steady decrease in the tensile bond strength of the interface, results in a decrease in critical energy release rate of the interface relative to the material of the layers. The G_{intc} corresponding to the tensile strength of the interface of 1.65 MPa, is adequate to provide crack growth perpendicular to the interface. A decrease in the tensile strength of the interface to 0.9 MPa in the 9-minute interface produces a decrease in the G_{intc} and the condition for the crack branching given in Equation 3 is satisfied. The crack is singly-deflected at the interface. The crack then kinks back into the layer immediately above the 9-minute inetrface.

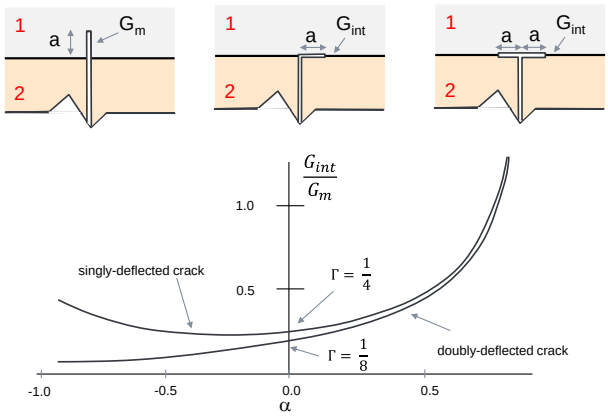

Figure 4: Crack penetration and deflection at an interface.

originated at the notch location when the load reached 5.2 kN, corresponding to Point -1 in the load response. The crack propagated vertically up to the 20-minute interface. The stable crack growth in the second printed layer resulted in a peak load of 8.0 kN. After reaching its initial peak load, the strain contours (ε_{xx}) showed strain localization at the weak interface between Points 1 and 2 in the load response. The ε_{xx} strain contours demonstrated that the crack branched into the third printed layer and continued to grow stably until reaching the second peak load. With further load increase, the crack propagated vertically through the third and consecutive layers, starting from the shifted point. The subsequent fracture load response closely resembled that of the 0-minute specimen, as the crack rapidly propagated across multiple inter-layer interfaces, in the post-peak stage.

The influence of further decrease in the tensile interface bond capacity in the 20-minute interface was evaluated for fracture across the interface. Figure.4 presents the typical fracture test response of the 20-minute beam and the ε_{xx} and strain contours at various points during the load response. The strain contours in ε_{yy} direction are also plotted at the corresponding load points for evaluation. Initially, the crack

The strain contours (ε_{yy}) at Points 1 and 2 indicated that the crack was deflected along the weak interface, continuing to grow along interface, showing a load decrease immediately after the initial peak load. As the CMOD increased, the load also increased beyond Point 2, resulting in a second peak load of 8.0 kN. Further the decrease in the interface fracture energy due to the weaker bond in the 20-minute interfaece produces a doubly-deflected crack. This indicates that the decrease in the tensile strength in the 20-minute specimen rsulted in the condition for the doubly-deflected crack at the interface.

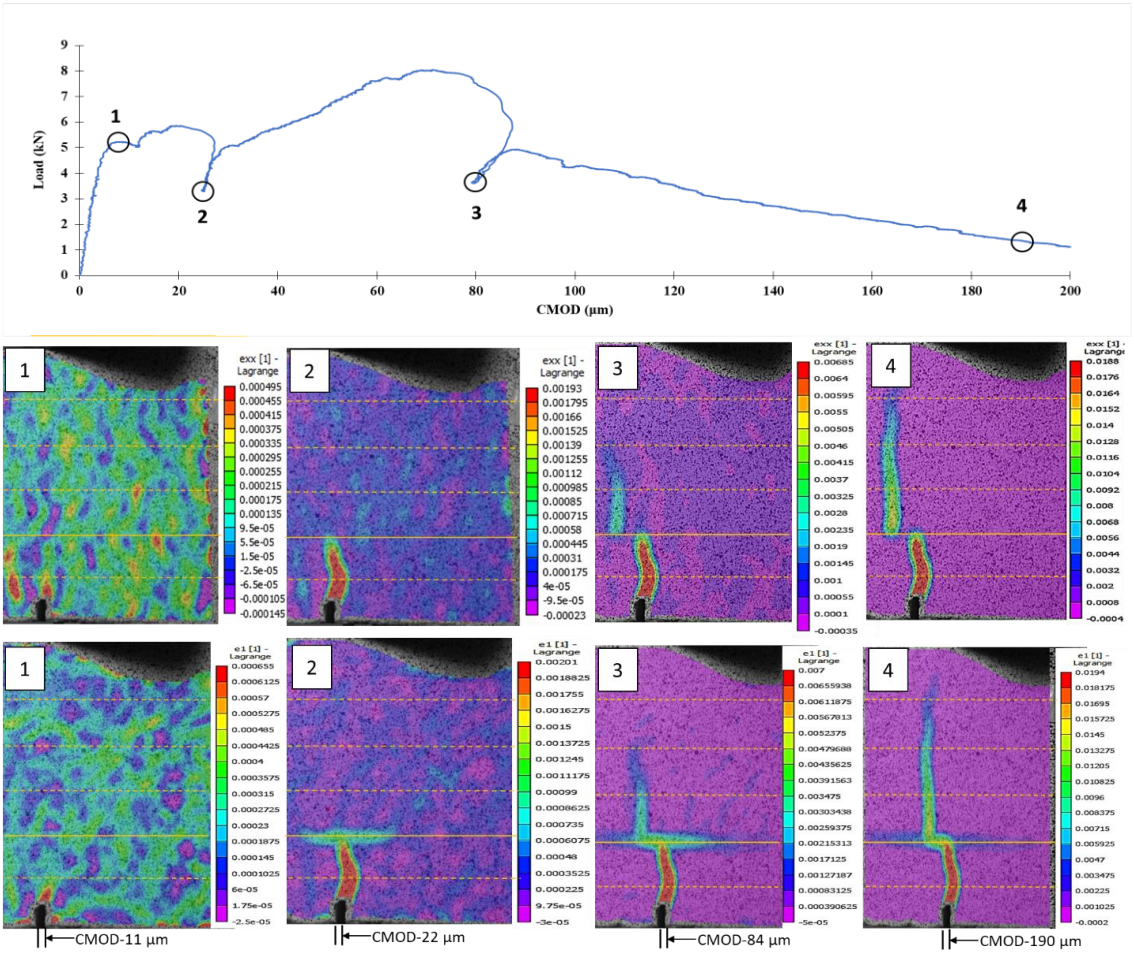

Fig.4. Load – CMOD response along with strain contours from the 20-minute specimen. The strain contours ε_{xx} and ε_{yy} are shown at different points in the load response.

The fracture behavior observed in the 0-minute printed beams closely resembles that of a homogeneous beam, with no transition of crack between layers. In contrast, the specimens printed with a time gap exhibited a notable deviation of crack from its original path, which can be attributed to the formation of a cold joint resulting from the presence of a weakened interface caused by the time gap between layers. There is a significant reduction in the overall crack opening due to the weak interface present in the crack path, that lead to significant crack deflection. Although the peak lead of the 0-minute and 20-minute beams were relatively similar when tested at different ages, a notable disparity was observed in their maximum crack opening in the fracture response, as the residual load decreased to 1 kN at around around 330 μm and 200 μm in the 0-minute and 20-minute beams, respectively.

The crack propagation in a layered structures not only depends on the toughness of the material but also the interface toughness which is a function of bond strength. The crack path in the 0-minute beams indicates that the toughness at

the interface is either equal to or higher than that of the material in the printed layers, confirming its behavior being similar to a homogeneous element, having a good bonding between successive layers in the printed assembly. The study revealed that the a 20-minute print time gap caused a weak interface between layers, showing the path of the least resistance for the crack propagation being in horizontal direction which lead to branching of crack into interface. The crack branching is produced due to low fracture toughness of the interface in 20-minute interval though the print time gap is significantly lower than the initial setting time of cement mix. Hence the cold joint is likely to be influenced by factors such as flocculation and agglomeration inside the material that cause internal structuration, but not the chemical aging and irreversible structural build-up within the material resulted by the setting time. Additionally, plastic shrinkage in the deposited material within the 20-minute interval lead to local surface drying, which further influenced the bond with the subsequent layer. Overall, the 20-minute time gap between printed layers resulted in a cold joint with poor bonding and low fracture toughness, adversely affecting the overall integrity of the element.

CONCLUSIONS

The fracture behavior of an extrusion-based 3D printed element is significantly influenced by the inter-layer interfaces which affect its homogeneity. The effect of the weak interface on the fracture behavior, essentially on crack propagation phenomena is studied by introducing print time gap between layers and performing three point bending test and digital image correlation studies. The following are the key findings of the research.

1. 3D printed specimens clearly demonstrated anisotropy induced because of layered structure, displaying varying strengths in three different directions, ranked in decreasing order: along the printed layers' direction, along the height of the element, and parallel to the printed layers.
2. A lesser or no time gap between the printed layers can ensure proper bonding between the adjacent layers of the printed structure, achieving a good composite action by complete vertical crack propagation along the depth.
3. An increased print time gap between the layers influences the bonding and the fracture behavior, demonstrating a deviated crack propagation horizontally at the interface.
4. The time gap between layers has a substantial influence on the fracture behavior, despite the interval being much shorter than the initial setting time of cement.
5. Careful evaluation of the fracture behavior in 3D printed structures is essential, taking into account various factors such as the print time gap that may lead to the weak interlayer interfaces.

ACKNOWLEDGEMENTS

We thank Simpliforge Creations, Siddipet, Telangana, India, for printing and supplying the samples.

REFERENCES

[1] Van Mier, J.G.M., 1997. *Fracture Processes of Concrete*. CRC Press.

[1] Freethink. (2023, March 8). 3D-printing houses. Retrieved July 25, 2023, from https://www.freethink.com/hard-tech/3d-printing-houses

[2] T.A.M. Salet, Z.Y. Ahmed, F.P. Bos, H.L.M. Laagland, 3D printed concrete bridge, in: Proceedings of the International Conference on Progress in Additive

Manufacturing, Pro-AM, 2018: pp. 2–9. https://doi.org/10.25341/D4530C.

[3] Guan, J., Wang, L., & Ma, G. (2022). Performance evaluation of reinforced concrete beam with 3d-printed permanent formwork. SSRN Electronic Journal, doi:10.2139/ssrn.4117121

[4] Skanska Claims Industry-First 3D-Printed Cladding. (2023, February 14). Construction Management, co.uk. Retrieved from https://constructionmanagement.co.uk/skanska-claims-industry-first-3d-printed-cladding/

[5] G. Vantyghem, W. De Corte, E. Shakour, O. Amir, 3D printing of a post-tensioned concrete girder designed by topology optimization, Autom Constr. 112 (2020). https://doi.org/10.1016/j.autcon.2020.103084.

[6] Y.W.D. Tay, J.H. Lim, M. Li, M.J. Tan, Creating functionally graded concrete materials with varying 3D printing parameters, Virtual Phys Prototyp. 17 (2022) 662–681. https://doi.org/10.1080/17452759.2022.2048521.

[7] R.J.M. Wolfs, F.P. Bos, T.A.M. Salet, Hardened properties of 3D printed concrete: The influence of process parameters on interlayer adhesion, Cem Concr Res. 119 (2019) 132–140. https://doi.org/10.1016/j.cemconres.2019.02.017.

[8] S.A.O. Nair, S. Panda, M. Santhanam, G. Sant, N. Neithalath, A critical examination of the influence of material characteristics and extruder geometry on 3D printing of cementitious binders, Cem Concr Compos. 112 (2020). https://doi.org/10.1016/j.cemconcomp.2020.103671.

[9] L. Reiter, T. Wangler, N. Roussel, R.J. Flatt, The role of early age structural build-up in digital fabrication with concrete, Cem Concr Res. 112 (2018) 86–95. https://doi.org/10.1016/j.cemconres.2018.05.011.

[10] A. Kazemian, X. Yuan, E. Cochran, B. Khoshnevis, Cementitious materials for construction-scale 3D printing: Laboratory testing of fresh printing mixture, Constr Build Mater. 145 (2017) 639–647. https://doi.org/10.1016/j.conbuildmat.2017.04.015.

[11] A.S. Alchaar, A.K. Al-Tamimi, Mechanical properties of 3D printed concrete in hot temperatures, Constr Build Mater. 266 (2021). https://doi.org/10.1016/j.conbuildmat.2020.120991.

[12] V.N. Nerella, S. Hempel, V. Mechtcherine, Effects of layer-interface properties on mechanical performance of concrete elements produced by extrusion-based 3D-printing, Constr Build Mater. 205 (2019) 586–601. https://doi.org/10.1016/j.conbuildmat.2019.01.235.

[13] Y. Zhang, Y. Zhang, L. Yang, G. Liu, Y. Chen, S. Yu, H. Du, Hardened properties and durability of large-scale 3D printed cement-based materials, Materials and Structures/Materiaux et Constructions. 54 (2021). https://doi.org/10.1617/s11527-021-01632-x.

[14] G.M. Moelich, J. Kruger, R. Combrinck, Plastic shrinkage cracking in 3D printed concrete, Compos B Eng. 200 (2020). https://doi.org/10.1016/j.compositesb.2020.108313.

[15] A. Cicione, J. Kruger, R.S. Walls, G. Van Zijl, An experimental study of the behavior of 3D printed concrete at elevated temperatures, Fire Saf J. 120 (2021). https://doi.org/10.1016/j.firesaf.2020.103075.

[16] N. Roussel, H. Bessaies-Bey, S. Kawashima, D. Marchon, K. Vasilic, R. Wolfs, Recent advances on yield stress and elasticity of fresh cement-based materials, Cem Concr Res. 124 (2019). https://doi.org/10.1016/j.cemconres.2019.105798.

[17] Otsubo, Y., Miyai, S., & Umeya, K. (1980). Time-dependent flow of cement pastes. Cement and Concrete Research, 10(4), 425-433.

[18] B. Panda, S.C. Paul, N.A.N. Mohamed, Y.W.D. Tay, M.J. Tan, Measurement of

tensile bond strength of 3D printed geopolymer mortar, Measurement (Lond). 113 (2018) 108–116. https://doi.org/10.1016/j.measurement.2017.08.051.

[19] Y. Weng, M. Li, D. Zhang, M.J. Tan, S. Qian, Investigation of interlayer adhesion of 3D printable cementitious material from the aspect of printing process, Cem Concr Res. 143 (2021). https://doi.org/10.1016/j.cemconres.2021.106386.

[20] T. Wangler, E. Lloret, L. Reiter, N. Hack, F. Gramazio, M. Kohler, M. Bernhard, B. Dillenburger, J. Buchli, N. Roussel, R. Flatt, Digital concrete: Opportunities and challenges, RILEM Technical Letters. 1 (2016) 67–75. https://doi.org/10.21809/rilemtechlett.2016.16.

[21] D. Asprone, F. Auricchio, C. Menna, V. Mercuri, 3D printing of reinforced concrete elements: Technology and design approach, Constr Build Mater. 165 (2018) 218–231. https://doi.org/10.1016/j.conbuildmat.2018.01.018.

[22] T.A.M. Salet, Z.Y. Ahmed, F.P. Bos, H.L.M. Laagland, Design of a 3D printed concrete bridge by testing*, Virtual Phys Prototyp. 13 (2018) 222–236. https://doi.org/10.1080/17452759.2018.1476064.

[23] PADT. (2022, April 12). Technology Behind the Tempe AZ 3D Printed House – a Habitat for Humanity First. PADTinc.com. https://www.padtinc.com/2022/04/12/technology-behind-the-tempe-az-3d-printed-house-a-habitat-for-humanity-first/

[24] E. Keita, H. Bessaies-Bey, W. Zuo, P. Belin, N. Roussel, Weak bond strength between successive layers in extrusion-based additive manufacturing: measurement and physical origin, Cem Concr Res. 123 (2019). https://doi.org/10.1016/j.cemconres.2019.105787.

[25] H. Kloft, H.W. Krauss, N. Hack, E. Herrmann, S. Neudecker, P.A. Varady, D. Lowke, Influence of process parameters on the interlayer bond strength of concrete elements additive manufactured by Shotcrete 3D Printing (SC3DP), Cem Concr Res. 134 (2020). https://doi.org/10.1016/j.cemconres.2020.106078.

[26] Y. Chen, K. Jansen, H. Zhang, C. Romero Rodriguez, Y. Gan, O. Çopuroğlu, E. Schlangen, Effect of printing parameters on interlayer bond strength of 3D printed limestone-calcined clay-based cementitious materials: An experimental and numerical study, Constr Build Mater. 262 (2020). https://doi.org/10.1016/j.conbuildmat.2020.120094.

[27] J.G. Sanjayan, B. Nematollahi, M. Xia, T. Marchment, Effect of surface moisture on inter-layer strength of 3D printed concrete, Constr Build Mater. 172 (2018) 468–475. https://doi.org/10.1016/j.conbuildmat.2018.03.232.

[28] Y.W.D. Tay, G.H.A. Ting, Y. Qian, B. Panda, L. He, M.J. Tan, Time gap effect on bond strength of 3D-printed concrete, Virtual Phys Prototyp. 14 (2019) 104–113. https://doi.org/10.1080/17452759.2018.1500420.

[29] Indian Standards Institution. (2013). Ordinary Portland cement, 53 grade - specification (BIS IS 12269 : 2013). New Delhi, India: Bureau of Indian Standards.

[30] Indian Standards Institution. (1970). SPECIFICATION FOR COARSE AND FINE AGGREGATES FROM NATURAL SOURCES FOR CONCRETE (Second Revision). Cement and Concrete Sectional Committee. Retrieved from https://law.resource.org/pub/in/bis/S03/is.383.1970.pdf

[31] Bureau of Indian Standards. (1988). Methods of physical tests for hydraulic cement, Part 5: Determination of initial and final setting times. IS 4031-5. New Delhi, India: BIS.

[32] European Committee for Standardization. (2005). Test method for metallic fibre concrete. Measuring the flexural tensile strength (limit of proportionality (LOP), residual). EN 14651:2005+A1:2007.

[33] Indian Standard. (1999). Splitting tensile

strength of concrete - Method of test. Bureau of Indian Standards. Retrieved from https://law.resource.org/pub/in/bis/S03/is.5816.1999.pdf